

**SURFACE SULFONATES LOCK SERUM ALBUMIN INTO A  
"HARD" CORONA**

Journal:	<i>Biomaterials Science</i>
Manuscript ID	BM-ART-03-2019-000475.R1
Article Type:	Paper
Date Submitted by the Author:	20-May-2019
Complete List of Authors:	Delgado, Jose; Florida State University, Chemistry & Biochemistry Surmaitis, Richard; Florida State University, Chemistry & Biochemistry Arias, Carlos; Florida State University, Chemistry & Biochemistry Schlenoff, Joseph; Florida State University, Chemistry & Biochemistry

# SURFACE SULFONATES LOCK SERUM ALBUMIN INTO A “HARD” CORONA

*Jose D. Delgado,<sup>¶</sup> Richard L. Surmaitis,<sup>¶</sup> Carlos J. Arias and Joseph B. Schlenoff<sup>\*‡</sup>*

Department of Chemistry and Biochemistry, Florida State University, Tallahassee, Florida  
32306

<sup>¶</sup> These authors contributed equally.

\* To whom correspondence should be addressed. E-mail: [schlen@chem.fsu.edu](mailto:schlen@chem.fsu.edu)

Department of Chemistry and Biochemistry.

**KEYWORDS:** polyelectrolyte, multilayer, biocompatible, thin film, nonfouling, TCP, tissue culture plastic

## ABSTRACT

The composition of the layer of proteins adsorbed to macro- or microscopic surfaces of synthetic origin influences the response of living systems to these materials. This adsorbed layer of proteins usually comprises a “soft” coating or corona of labile or exchangeable adsorbed proteins on top of a more tenaciously held “hard” corona in contact with the surface. Here, we link the dependence of cell adhesion on a 20 nm film of polyelectrolyte complex to the “hardness” of the initial corona using albumin, the most prevalent protein in serum. The ease with which albumin can be lost depends on the surface functional group - carboxylate or sulfonate, in particular aromatic sulfonate. Carboxylate permits easier loss of albumin, which presumably allows the subsequent adsorption of proteins such as fibronectin, required for cell adhesion. Sulfonate holds on to albumin more strongly, producing a persistent hard corona likely to remain biocompatible. The mechanism is thought to be related to the higher energy of interaction between sulfonate and amine than between carboxylate and amine, and provides insight on possible reasons why so-called “tissue culture plastic” works so well for *in vitro* cell culture.

## INTRODUCTION

Any materials, such as implants and scaffolds, applied for extended use in living organisms must be compatible with their location and duration of use. The surface of a material in contact with a biological fluid quickly acquires a coating of proteins. This coating or corona of proteins controls many subsequent events, such as cell adhesion and proliferation, thrombosis, and inflammation.<sup>1</sup> The dynamic nature of protein adsorption, recognized by Vroman,<sup>2</sup> provides a constantly shifting surface composition. In contact with blood, the initial makeup of the corona is thought to include proteins in higher concentration, notably serum albumin. A “soft” or exchangeable corona is believed to decorate a more persistent “hard” corona comprised of more tenacious proteins attached directly to the surface.<sup>3</sup>

Vroman’s findings regarding the changing protein composition on planar surfaces were recognized decades later as essential for understanding the fate of nanoparticles circulating in the bloodstream.<sup>4 5</sup> For nanoparticles, the suppression of nonspecific protein adsorption is sought so that circulating particles do not agglomerate or become tagged for removal (e.g. by phagocytes) before they reach their intended target.<sup>6</sup> On planar surfaces, extremes of cell adhesion, from “cell repelling” to optimal cell adhesion, are desired.<sup>7</sup>

In parallel with investigations on the composition and influence of adsorbed proteins have come intensive efforts to suppress such adsorption as much as possible, providing “stealth” coatings that allow nanoparticles to circulate and planar surfaces to remain unfouled.<sup>8</sup> PEGylation, or coating with oligomeric or polymeric ethylene glycol to reduce nonspecific adsorption, has been practiced for many years.<sup>9</sup> More recent interest has focused on zwitterionic coatings, thought to mimic the nonfouling properties of the cell membrane.<sup>10</sup> However, it is becoming increasingly apparent that even “stealth” coatings are not fully effective in preventing protein adsorption<sup>11, 12</sup> and a strategy is evolving to control and/or exploit the inevitable corona.<sup>13-15</sup>

There has been much interest, for many years, in preparing a rugged passivating layer of albumin on surfaces to decrease platelet attachment for example, by either spontaneously adsorbing albumin<sup>16</sup> or immobilizing albumin on a surface using covalent bonds<sup>17</sup> or antibodies to albumin,<sup>18</sup> as well as conjugating albumin to therapeutics for extended circulation.<sup>19</sup> One of the very few nanoparticles FDA-approved for therapy consists of the anticancer drug paclitaxel bound to 130 nm albumin clusters (Abraxane™).<sup>20</sup> Recently, Peng et al. elaborated on the benefits of a preformed albumin coating for nanoparticle drug delivery systems.<sup>21</sup> They showed that a physically adsorbed layer of albumin reduced the toxicity, decreased IgG and complement activation, prolonged the circulation time, and reduced phagocytosis of nanoparticles *in vitro* and

*in vivo*. Li et al. have demonstrated similar low-immunogenic albumin coatings for tumor-targeting nanoparticles.<sup>22</sup>

Protein adsorption/corona formation, an extremely complex topic,<sup>23</sup> depends on numerous variables, some which are controlled, some not controlled (or perhaps not recognized). Thus, studies of protein adsorption and cell adhesion to surfaces are aided by experimental systems that control as many variables as possible, including the sign and density of the surface charge, polarity, and hydrophobicity. Well-defined monolayers formed by the spontaneous adsorption of alkanethiols on gold are useful substrates in this respect.<sup>24</sup> Versatile coatings incorporating (poly) phenolic residues such as polydopamine have stimulated much recent exploration into methods to isolate physiological systems from artificial substrates.<sup>25, 26</sup> Polyelectrolyte multilayers, PEMUs, thin films of polyelectrolyte complex assembled by the alternating exposure of a planar or nanoparticle surface to polycations and polyanions, also offer a great deal of control over surface variables.<sup>27</sup> The numerous combinations of polyelectrolytes employed to study protein adsorption and cell adhesion<sup>28</sup> on PEMUs have been extensively reviewed (but rarely compared).<sup>29, 30</sup> Of the commercially available synthetic polyelectrolytes the most-used polyanions,  $\text{Pol}^-$ , in PEMUs are the sodium salt of poly(acrylic acid), PAA, and poly(styrene sulfonate), PSS. On the polycation,  $\text{Pol}^+$ , side, poly(allylamine hydrochloride), PAH, and poly(diallyldimethylammonium chloride), PDADMAC, are common.

Almost all PEMUs are “hydrophilic” in the sense that they have relatively low contact angles,<sup>31, 32</sup> unless they have been designed otherwise, and they contain a substantial amount of water.<sup>33</sup> Interactions between surface and protein are thus believed to be mainly due to ion pairings between surface and protein charges (i.e. “electrostatic” interactions).<sup>10, 34</sup> Although net charge density is generally known to be crucial in protein adhesion,<sup>35, 36</sup> it is not generally acknowledged that the chemical identity of the charge itself plays an important role (“a charge is a charge”). In the present study, cell adhesion and spreading were evaluated on PEMUs terminated with two chemically distinct kinds of polyanions. Included in our study are random copolymers with mixtures of carboxylate and sulfonate functionality or with zwitterionic repeat units known to reduce/eliminate both protein adsorption and cell attachment.<sup>37</sup> Cell response was correlated to the robustness of albumin adhesion to the surfaces comprising different functionality.<sup>14</sup>

## EXPERIMENTAL METHODS

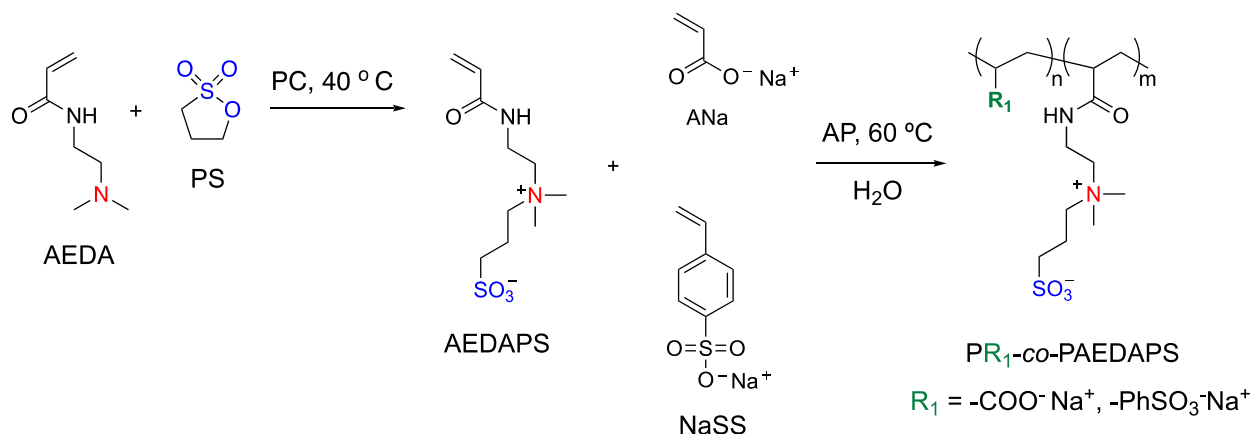
**Materials.** Poly(allylamine hydrochloride) (PAH, 40 wt%,  $M_w$  120,000 – 200,000 g mol<sup>-1</sup>), poly(vinylsulfonic acid, sodium salt) (PVS, 25 wt% in water  $M_w$  4,000 – 6,000 g mol<sup>-1</sup>), and

poly(acrylic acid) ( $M_w$  240,000 g mol<sup>-1</sup>) were obtained from Polysciences; 3-[2-(acrylamido)-ethyltrimethylammonio]propane sulfonate (AEDAPS) was synthesized as described previously;<sup>38, 39</sup> sodium acrylate (ANa, 97%), propylene carbonate anhydrous (PC, 99%), bovine serum albumin, BSA, in lyophilized powder form, sodium bicarbonate and 1,3-propane sultone (PS, 99%) were from Sigma-Aldrich; sodium 4-vinylbenzenesulfonate (NaSS, purity  $\geq$  90% Aldrich) was purified by recrystallization from water to a monomer purity of  $>98\%$ ; poly(sodium 4-styrenesulfonate) (PSS,  $M_w$  70,000 g mol<sup>-1</sup>), obtained from Scientific Polymer Products, was purified by dialysis then dried by lyophilization; ammonium persulfate (AP, 98% Aldrich) was recrystallized twice from deionized water; deuterium oxide was from Cambridge Isotope Laboratories; Cosmic Calf serum was from Thermo Scientific; 3T3-Swiss albino fibroblasts were initially purchased from American Type Culture Collection as ATCC CCL-92 cells and maintained in the laboratory for numerous generations; gentamicin was from Invitrogen. Deionized water (18 M $\Omega$  cm, Milli-Q) was used for all aqueous solutions. Trizma<sup>®</sup> base (Sigma,  $\geq$  99%), Trizma<sup>®</sup> hydrochloride (Sigma,  $\geq$  99%) and NaCl (Sigma,  $\geq$  99.5%) were used as received. <sup>14</sup>C-tetraethylammonium, 0.25 mCi, as the bromide salt, half-life 5730 y,  $E_{max} = 0.156$  MeV ( $\beta$ -emitter) with a specific activity of 185 Ci mol<sup>-1</sup> and Na<sup>125</sup>I, 1 mCi, with a concentration of 100 mCi mL<sup>-1</sup>, and <sup>125</sup>I-labeled BSA (1.1 mCi mg<sup>-1</sup>) were obtained from PerkinElmer Radiopharmaceuticals. Cell experiments were performed on flat bottom, 12-well plates (Jet-Biofil, Tissue Culture Products).

**Polymerizations monitored by <sup>1</sup>H-NMR.** Copolymerization kinetics of the NaSS/ANa monomers were followed directly in NMR tubes at 60.0 °C in a 500 MHz Bruker AM 500 spectrometer (Figure S1). The spectrometer had a 5 mm <sup>1</sup>H selective probe controlled with a calibrated BVT 1000 temperature unit. In a separate flask, monomers NaSS (0.1 g, 0.47 mmol) and ANa (0.045 g, 0.47 mmol) were mixed in D<sub>2</sub>O (1.19 mL) and purged with N<sub>2</sub> for 40 min. Then the ammonium persulfate initiator 0.1 wt% was introduced in the NMR tube and it was purged with N<sub>2</sub> for 30 min. The monomer solution was then transferred to the NMR tube with a syringe and maintained in an ice bath before starting the polymerization. The spectrometer was preheated at 60 °C, the NMR tube was introduced to the spectrometer and the first spectrum was taken and designated as time = 0 of the polymerization. Spectra were recorded every 10 min for one h, wherein all polymerizations were carried to a conversion of  $< 50\%$  to minimize composition drift.

Polymers were: poly(sodium 4-styrenesulfonate-co-3-[2-(acrylamido)-ethyltrimethylammonio]propane sulfonate), [PSS<sub>n</sub>-co-PAEDAPS<sub>m</sub>], poly(sodium acrylate-co-3-[2-(acrylamido)-ethyltrimethylammonio]propane sulfonate), [PAA<sub>n</sub>-co-PAEDAPS<sub>m</sub>] and poly(sodium 4-styrenesulfonate-co-sodium acrylate), [PSS<sub>n</sub>-co-PAA<sub>m</sub>].

**Synthesis of PAA<sub>n</sub>-co-PAEDAPS<sub>m</sub> and PSS<sub>n</sub>-co-PAEDAPS<sub>m</sub>.** A typical copolymerization of PAA<sub>0.5</sub>-co-PAEDAPS<sub>0.5</sub> started with 12 mL of water in a 100 mL three-neck round-bottom flask under flowing N<sub>2</sub>. AEDAPS (2.0 g, 7.56 mmol), sodium acrylate (0.71 g, 7.57 mmol) and ammonium persulfate (2.7 mg, 0.1 wt%) were then added. The solution was heated at 60 °C and it was allowed to react under N<sub>2</sub> for 45 min. The product was cooled and dialyzed against water (using Spectra/Por 12,000 - 14,000 molecular weight cutoff, MWCO, tubing) for 40 h. The purified polymer was freeze-dried as a light yellow powder. <sup>1</sup>H NMR (600 MHz, D<sub>2</sub>O): 3.67 (br s), 3.46 (br d), 3.14 (s), 2.94 (t), 2.21 (br), 2.06 (br), 1.9-1.4 (br m). The synthesis of PSS<sub>0.5</sub>-co-PAEDAPS<sub>0.5</sub> was conducted under similar conditions with 2.8 g (11.97 mmol) of NaSS and 3.17 g (11.99 mmol) of AEDAPS with 0.1 wt % ammonium persulfate based on total monomer. Samples were freeze-dried for 2 days and finally dried under vac for 60 h at 110 °C in order to remove all absorbed water and to ensure accurate concentrations of polymer solutions. <sup>1</sup>H-NMR confirmed the absence of residual monomer. <sup>1</sup>H NMR (600 MHz, D<sub>2</sub>O): 7.95-7.31 (2 H), 7.26 – 6.21 (2H), 3.66 – 3.54 (br ), 3.53 – 3.40 (br ), 3.38 – 3.20 (br) 3.05 – 2.78 (br) 2.32 – 2.01 (br ), 1.99 – 0.99 (6H) ppm. (Supporting information, Figure S2 D-G).



**Scheme 1.** Synthesis of the monomer AEDAPS and copolymers: PAA<sub>n</sub>-co-PAEDAPS<sub>m</sub> and PSS<sub>n</sub>-co-PAEDAPS<sub>m</sub>.

**Synthesis of PSS<sub>0.5</sub>-co-PAA<sub>0.5</sub>.** In a round-bottomed flask sodium acrylate (1.13 g, 12.0 mmol) and sodium 4-styrenesulfonate (2.81 g, 12.0 mmol) were dissolved in 13 mL of water. The solution was degassed and the initiator, ammonium persulfate (34 mg, 0.149 mmol), was added. The polymerization was performed for 40 min under N<sub>2</sub> with stirring at 60 °C. The polymer was purified by dialysis against water (Spectra/Por, MWCO 12,000 – 14,000) and recovered by freeze-drying to yield a white product. <sup>1</sup>H NMR (600 MHz, D<sub>2</sub>O): 7.95 – 7.31 (2 H), 7.26 – 6.21 (2H), and 2.5 – 1.0 (6H) ppm. (Supporting information, Figure S2 H).

**Table 1.** Properties of polyelectrolytes determined by NMR and SEC-MALLS

Polyelectrolyte	f <sup>a</sup>	F <sup>b</sup>	Conversion (%)	$M_w \times 10^{-5}$ (g mol <sup>-1</sup> ) <sup>c</sup>	$M_w/M_n$ <sup>c</sup>	$dn/dc$ (mL/g) <sup>c</sup>
PSS	100	100	49.5	3.25	1.91	0.175
PAA	100	100	-	2.40	-	-
PVS	100	100	-	0.04 – 0.06 <sup>d</sup>	-	-
PAH	100	100	-	1.2-2.0 <sup>d</sup>	-	-
PSS- <i>co</i> -PAA	50	50.5	47.5	2.40	2.23	0.177
PSS- <i>co</i> -PAEDAPS	50	51.5	46.3	2.80	2.03	0.182
	75	74.6	44.2	2.45	1.98	0.180
PAA- <i>co</i> -PAEDAPS	50	52.3	43.2	3.02	1.84	0.172
	75	75.2	52.1	2.73	1.80	0.176

<sup>a</sup>mole% feed<sup>b</sup>mole% in polymer by NMR<sup>c</sup>Determined by SEC-MALLS in NaNO<sub>3</sub> 0.2 M at 25 °C.<sup>d</sup>from supplier

**<sup>1</sup>H NMR.** Copolymers were analyzed by <sup>1</sup>H-NMR (Avance-600 MHz, Bruker) using D<sub>2</sub>O as the solvent. Compositions of copolymers PAA-*co*-PAEDAPS and PSS-*co*-PAEDAPS were calculated from the proton peak areas.

**Size Exclusion Chromatography (SEC).** Absolute number-average molar mass ( $M_n$ ), weight-average molar mass ( $M_w$ ), and dispersity ( $D = M_w/M_n$ ) of polymers were determined using size exclusion chromatography with three SEC columns 17 μm (30 x 7.5 mm, Tosoh Biosciences TSK-GEL G5000PW) in series using a TSK guard column, then a DAWN-EOS light scattering detector ( $\lambda = 690$  nm) previously calibrated with toluene and an interferometric refractometer, both from Wyatt Technologies. The concentration of polymer solution injected was 1.0 mg mL<sup>-1</sup> in 0.2 M NaNO<sub>3</sub> and the flow rate was 0.5 mg mL<sup>-1</sup>. All mobile phases were maintained at 25 °C. Poly(sodium 4-styrenesulfonate) standards from Scientific Polymer Products Inc. were used to check the performance of the instrument. Detectors at various angles were normalized with BSA. Data were analyzed using ASTRA 5.3.4 software from Wyatt technology. The specific refractive index increment,  $dn/dc$ , was determined on the OPTILAB-DSP calibrated with NaCl solutions of known refractive indexes. SEC chromatograms are shown in Figure S3.

**Polyelectrolyte Multilayer Buildup.** Polyelectrolyte solutions were made in Tris buffer (10 mM Tris, 0.15 NaCl M) at pH 7.4. Multilayers on Si were built manually on double side polished silicon 100 wafers (Okmetic,  $381 \pm 12 \mu\text{m}$  thick,  $125 \pm 0.5 \text{ mm}$  diameter). The silicon wafers were cleaned using “piranha” solution (70%  $\text{H}_2\text{SO}_4$ /30%  $\text{H}_2\text{O}_2$ , **Caution!** *Piranha is very corrosive and extreme care should be taken when handling it*) for 15 min at room temp then washed vigorously with water and dried under a jet of  $\text{N}_2$ . The dipping time of the polymer solutions (1.0 mM) was 10 min which was followed by 3 x (1 min) rinsing steps in deionized water.

**Polyelectrolyte Multilayers on Tissue Culture Plastic (TCP).** Cell culture experiments were performed on PEMUs using TCP plates as the substrate.<sup>40</sup> TCP plates were provided by the manufacturer cleaned, sterile and sealed, where the surface was treated with a plasma, according to the manufacturer, which provides negative charges on the surface. For multilayer assembly, TCPs were immersed into 1000 mL beakers containing polyelectrolyte solutions. After the coating was complete the TCPs were dried and sterilized for 5 min using a UV lamp. The seeding of cells was done immediately after the TCPs were coated with the PEMU.

**PEMU nomenclature:** [A/B]<sub>n</sub>X indicates a multilayer containing “n” bilayers of polycation A and polyanion B, starting with A. The PEMUs used for this study were: [PAH/PAA]<sub>4.5</sub>X, [PAH/PSS]<sub>4.5</sub>X where X is the terminating polyelectrolyte layer. [X = PAA, PSS, PVS, PAA<sub>n</sub>-co-PAEDAPS<sub>m</sub>, PSS<sub>n</sub>-co-PAEDAPS<sub>m</sub> and PSS<sub>0.5</sub>-co-PAA<sub>0.5</sub>].

Film thicknesses on Si were measured with an ellipsometer (Gaertner L116S) using a 632.8 nm laser at 70° incidence angle. A refractive index of 1.55 was used for multilayers.

**Cell Culture.** 3T3 fibroblasts were cultured in Dulbecco’s Modified Eagle’s medium supplemented with 1 g L<sup>-1</sup> L-glutamine, 1.2 g L<sup>-1</sup> NaHCO<sub>3</sub>, 10% cosmic calf serum, 100 U mL<sup>-1</sup> penicillin G, 100 μg mL<sup>-1</sup> streptomycin, 0.25 μg mL<sup>-1</sup> amphotericin B, and 10 μg mL<sup>-1</sup> gentamicin. Cells were incubated at 37 °C with 5% CO<sub>2</sub> (Nu-4750, NuAire). Uncoated 6- or 12-well TCP plates were used as controls.

**Microscopy and Live Cell Imaging.** Live cell imaging was performed to observe the behavior of cells for 3 days. PEMUs for these experiments were assembled in 35 mm TCP dishes using the same conditions that were used with silicon wafers. Images were obtained with a Nikon Ti-E inverted microscope and a Cool Snap HQ2 camera. These cells were controlled in a LiveCell chamber and incubated at 37 °C in 5% CO<sub>2</sub> at 60% relative humidity to avoid evaporation of the

media. Images were taken every 20 s for the first 3 h, followed by 1 min for the next 21 h and finally every 5 min for the following 48 h, for a total of 72 h of cell analysis.

**Radioactive Ion Assays.** The negative charge density of surfaces was measured using  $^{14}\text{C}$ -tetraethylammonium bromide, TEABr,  $3.5 \text{ Ci mol}^{-1}$  in 2.5 mL ethanol. 175  $\mu\text{L}$  of this solution was added to 49.8 mL of water to prepare 50 mL of  $1.0 \times 10^{-4} \text{ M}$  TEA. The concentration of  $^{14}\text{C}$ -TEABr, nominally  $1.0 \times 10^{-4} \text{ M}$ , was checked by measuring its conductivity with a conductivity meter (Thermo Scientific, Orion 3 Star) fitted with a miniature Pt conductivity probe. The conductivity was 5% higher than that of a  $1.0 \times 10^{-4} \text{ M}$  TEABr standard solution. The actual concentration of  $^{14}\text{C}$ -TEABr was  $1.05 \times 10^{-4} \text{ M}$ .

Samples (PEMUs on Si, bare Si, and bare TCP) were immersed in the  $1.05 \times 10^{-4} \text{ M}$   $^{14}\text{C}$ -TEABr solution then removed and dried with a jet of  $\text{N}_2$ . The dried sample with radiolabeled counterions was placed face down onto a piece of plastic scintillator (SCSN-81 Kuraray, 3 mm thick, 38 mm diameter, emission peak 437 nm), which rested on the end of an RCA 8850 photomultiplier tube, PMT, inside a black box. The PMT was biased to  $-2300 \text{ V}$  by a Bertran 313B power supply and connected to a Phillips PM6654C frequency counter/timer. Labview software utilized a gate time of 10 s and a pulse threshold of  $-20 \text{ mV}$  to collect the counts. Counts are reported as counts per second (cps). The background, subtracted from all readings, was typically 6 cps. A calibration curve was constructed by drying 1 to 5  $\mu\text{L}$  droplets of the  $^{14}\text{C}$ -TEABr solution on top of the scintillator.

**Protein Labeling and Assays.**  $^{125}\text{I}$ -labeled BSA was either purchased from Perkin Elmer or prepared in-house using the following procedure:  $[\text{Na}^{125}\text{I}]$  1 mCi was supplied in 10  $\mu\text{L}$   $1.0 \times 10^{-5} \text{ M}$  NaOH. This isotope was combined with 1.0 mL of PBS and added to 1.0 mL of  $2.0 \text{ mg mL}^{-1}$  of unlabeled bovine serum albumin (Sigma Aldrich). Three iodination beads (Thermo Scientific) were added to tag the BSA with  $^{125}\text{I}$ . The reaction mixture was diluted with 7.0 mL of PBS to yield 10.0 mL of  $0.2 \text{ mg mL}^{-1}$   $^{125}\text{I}$ -BSA solution of specific activity  $0.5 \text{ mCi mg}^{-1}$ . The solution was filtered with a  $0.1 \mu\text{m}$  filter and then dialyzed (Thermo Scientific, dialysis cassette, MWCO = 3,500) for 12 h.

Labeled protein was adsorbed to Si wafers coated with PEMUs with different terminating layers as well as pieces of TCP and untreated polystyrene (VWR). A lead spacer with a rectangular opening (1 mm thick, 2 mm x 5 mm opening) was placed between the substrate and the scintillator (EJ-256-5 Elgen Technology, 6.35 mm thick, 25.4 mm diameter, emission peak 425 nm) to prevent contamination of the scintillator and to define a constant area of sample

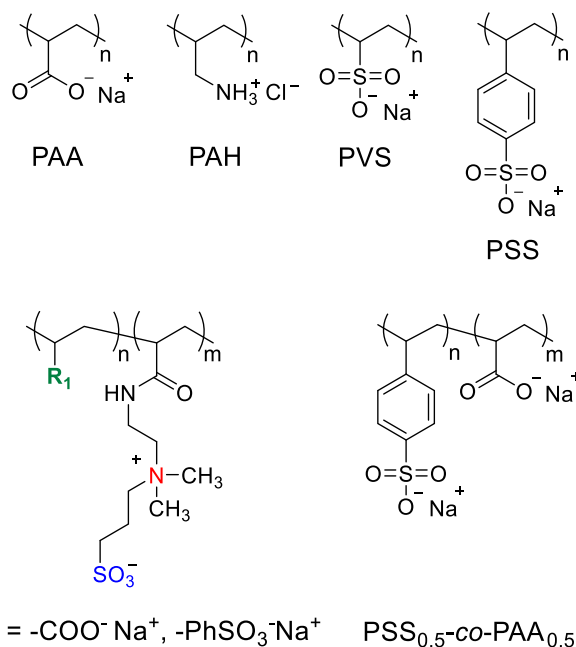
exposed for counting. Surfaces were first submerged into radiolabeled albumin solution for 30 min then rinsed in PBS and water. The samples were then placed on the scintillator.

Calibration curves (cps vs. mg of BSA) were prepared by drying 1.0 to 5.0  $\mu\text{L}$  droplets of the radiolabeled albumin solution on the surface of one side of a Si wafer. (Supporting information, Figure S4). The nmoles, or  $\mu\text{g}$ s, obtained were converted to  $\mu\text{moles m}^{-2}$  or  $\text{mg m}^{-2}$  using the open area of the spacer.  $[^{125}\text{I}]$ -BSA on Si wafer required a correction for counts coming from the back of the wafer because both sides of the samples were coated with PEMU and exposed to radiolabeled albumin (Figure S5). This correction was performed by drying 1.0 to 5.0  $\mu\text{L}$  droplets of the radiolabeled albumin solution on one side of the wafer. Counts were collected with this side facing toward and then away from the scintillator. All protein adsorption data points were collected in triplicate.

## RESULTS AND DISCUSSION

Cell attachment and spreading are used here to compare the response of a complex physiologically relevant system to the type of surface charge. The cell arrives at the interface long after the first proteins.<sup>41</sup> Membrane-bound integrins attach to specific sites (eg the Arg-Gly-Asp, RGD, motif) on adsorbed cell-adhesive proteins such as fibronectin and vitronectin, forming a preliminary “soft contact.” The “quality” of adhesion is reported in the case of many cells, such as the fibroblasts used here, not only by the density of attached cells but also by their morphology. If the adhesion protein is bound strongly enough to the surface, a poorly-understood “mechanotransduction” apparatus translates the tension of cytoskeletal fibers anchored to integrins, causing them to cluster, form more robust “focal adhesions,” and the cell spreads.<sup>42</sup>

The multilayers used here presented carboxyl or sulfonate anionic functional groups at their surfaces. The structures of polymers used in the present study are shown in Scheme 2. Zwitterionic repeat units are net neutral. Polycations ( $\text{Pol}^+$ ) are known to promote adhesion but also induce cytotoxicity if the positive charge density is too high.<sup>43</sup> PAH was used throughout as  $\text{Pol}^+$  for assembly. The primary amine functionality of PAH bears some resemblance to that of polylysine, which is used extensively in monolayer form (i.e. low charge density) to promote protein and cell adhesion.<sup>44</sup>



**Scheme 2.** Structures of polyelectrolytes used in this study.

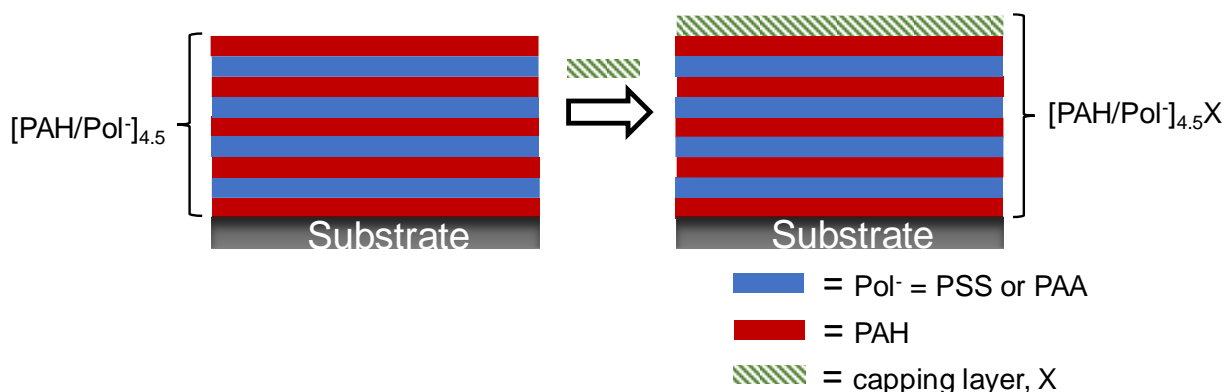
The use of a polyanion as a terminating layer may appear to be non-ideal for protein adsorption given the net negative charge of most proteins at physiological pH. However, it is well established that negatively charged proteins like serum albumin, with a net charge of -17 at physiological pH,<sup>45</sup> adsorb *via* positive patches.<sup>46</sup> Counterion release plays a central role in providing an (entropic) driving force for pairing between opposite charged units on a surface and protein, as described in the steric mass action model of Brooks and Cramer<sup>47</sup> and summarized recently by Xu et al. for protein/polyelectrolyte complexation.<sup>34</sup> For example, serum albumin adsorbs strongly on silica though the process is endothermic.<sup>48</sup> So-called “tissue culture plastic,” TCP, in which carboxylate groups are induced on the surface of polystyrene with a plasma,<sup>49, 50</sup> is widely used as a substrate for cell culture.

Ultrathin PEMUs of thickness < 20 nm were employed throughout to avoid effects of film modulus on cell attachment.<sup>51</sup> Finite element analysis on the effective modulus of a PEMU on glass<sup>52</sup> shows that the film thickness needs to approach several  $\mu\text{m}$  for a cell to be mechanically decoupled from the substrate.<sup>51</sup> In the <100 nm limit of thickness the effective modulus is in the GPa range<sup>52</sup> and it is assumed that PEMU surface properties dictate cell adhesion. For thicker, softer films, enhancing stiffness by crosslinking can promote cell attachment.<sup>29</sup> In the present work the number of layers was maintained at eight, which does not allow excess positive polyelectrolyte to accumulate within the PEMU.<sup>53</sup> We have shown that this excess charge can migrate to the surface and switch the surface charge from negative to positive.<sup>54</sup>

Copolymers prepared for this study all had molecular weights on the order of  $10^5$  and polydispersities around 2 (see Table 1). Conversions were maintained below 50% to avoid composition drift, and kinetics studies (see Supporting Information) indicated no significant difference in monomer reactivities (the mole fraction monomer incorporated into the copolymer was about the same as the mole fraction in solution). Thus, the copolymers were assumed to be close to random. PAA-co-PAEDAPS has been previously synthesized,<sup>55</sup> whereas PSS-co-PAEDAPS has not. The maximum mole fraction of zwitterionic monomer in PAEDAPS copolymers was 0.5 to prevent loss of polymer from the surface.<sup>55</sup>

### Protein adsorption: $[\text{PAH/PSS}]_{4.5}\text{X}$ versus $[\text{PAH/PAA}]_{4.5}\text{X}$

For adsorption studies, albumin was used as it is the most abundant protein in serum. The adsorption of serum albumin on PAH/PSS multilayers was initially reported by the Strasbourg group.<sup>56</sup> In the present work, two different “base” multilayers, each terminated in PAH, allowed variation of the capping (negative) layer. Scheme 3 depicts the sequence of layers combining a “base” of 9 layers, starting with PAH ( $[\text{PAH/PSS}]_{4.5}$  or  $[\text{PAH/PAA}]_{4.5}$ ), capped with layer X, to yield  $[\text{PAH/PSS}]_{4.5}\text{X}$  and  $[\text{PAH/PAA}]_{4.5}\text{X}$  PEMUs.



**Scheme 3.** Showing the construction of a “base” of 9 layers (4.5 bilayers) of PAH and PSS, or PAH and PAA, topped by a “capping layer” which was usually a negative polyelectrolyte, but in one instance was PAH (which required an additional Pol<sup>-</sup> layer). The layering structure is idealized, as adjacent Pol<sup>-</sup> and Pol<sup>+</sup> are interpenetrating.

The albumin was radiolabeled with  $^{125}\text{I}$ , causing minimal perturbation to the dimensions, composition and charge distribution of the protein. The  $^{125}\text{I}$  label typically appears on (neutral) tyrosine whereas labeling with large fluorescent dyes may interfere with adsorption.<sup>57</sup> Protein adsorption monitored with the quartz crystal microbalance gives significantly higher amounts,

although the relative surface coverages track those determined with radiolabeling and surface plasmon resonance.<sup>58</sup>

**Table 2.** Summary of surfaces and qualitative albumin adsorption and cell adhesion in this study

Base Multilayer	Thickness (nm) <sup>a</sup>	Capping layer	Capping Charge	Albumin adsorption <sup>c</sup>	Cell adhesion <sup>c</sup>
PAH/PAA	17.7 ± 0.2	PAH*	+	G	G
PAH/PAA	16.2 ± 0.3	PSS <sub>0.5</sub> -co-PAA <sub>0.5</sub>	-	G	G
PAH/PAA	17.1 ± 0.2	PAA <sub>0.5</sub> -co-PEDAPS <sub>0.5</sub>	-	P	P
PAH/PAA	16.9 ± 0.4	PAA <sub>0.75</sub> -co-PEDAPS <sub>0.25</sub>	-	P	P
PAH/PAA	16.7 ± 0.3	PAA	-	P	G
PAH/PAA	16.3 ± 0.1	PSS	-	G	P
PAH/PAA	16.5 ± 0.2	PVS	-	G	G
TCP	---	---	-	G	G
PAH/PSS	16.3 ± 0.8	PAH*	+	G	P
PAH/PSS	16.0 ± 0.4	PSS <sub>0.5</sub> -co-PAA <sub>0.5</sub>	-	G	G
PAH/PSS	16.3 ± 0.2	PSS <sub>0.5</sub> -co-PEDAPS <sub>0.5</sub>	-	P	P
PAH/PSS	15.9 ± 0.3	PSS <sub>0.75</sub> -co-PEDAPS <sub>0.25</sub>	-	G	P
PAH/PSS	15.5 ± 1.0	PSS	-	G	P
PAH/PSS	15.8 ± 0.4	PAA	-	---	G
PAH/PSS	15.7 ± 0.2	PVS	-	---	P
PAH/PVS	16.0 ± 0.3	PVS	-	G	P
CONTROL <sup>b</sup>	1.5 ± 0.05	---	-	G	---

<sup>a</sup> Dry thickness measured using ellipsometry before albumin adsorption. Films quickly swell by a factor of about 2 when immersed in buffer.

<sup>b</sup> native SiO<sub>2</sub> layer on silicon wafer

\* Positive charge surface (5.5 bilayers)

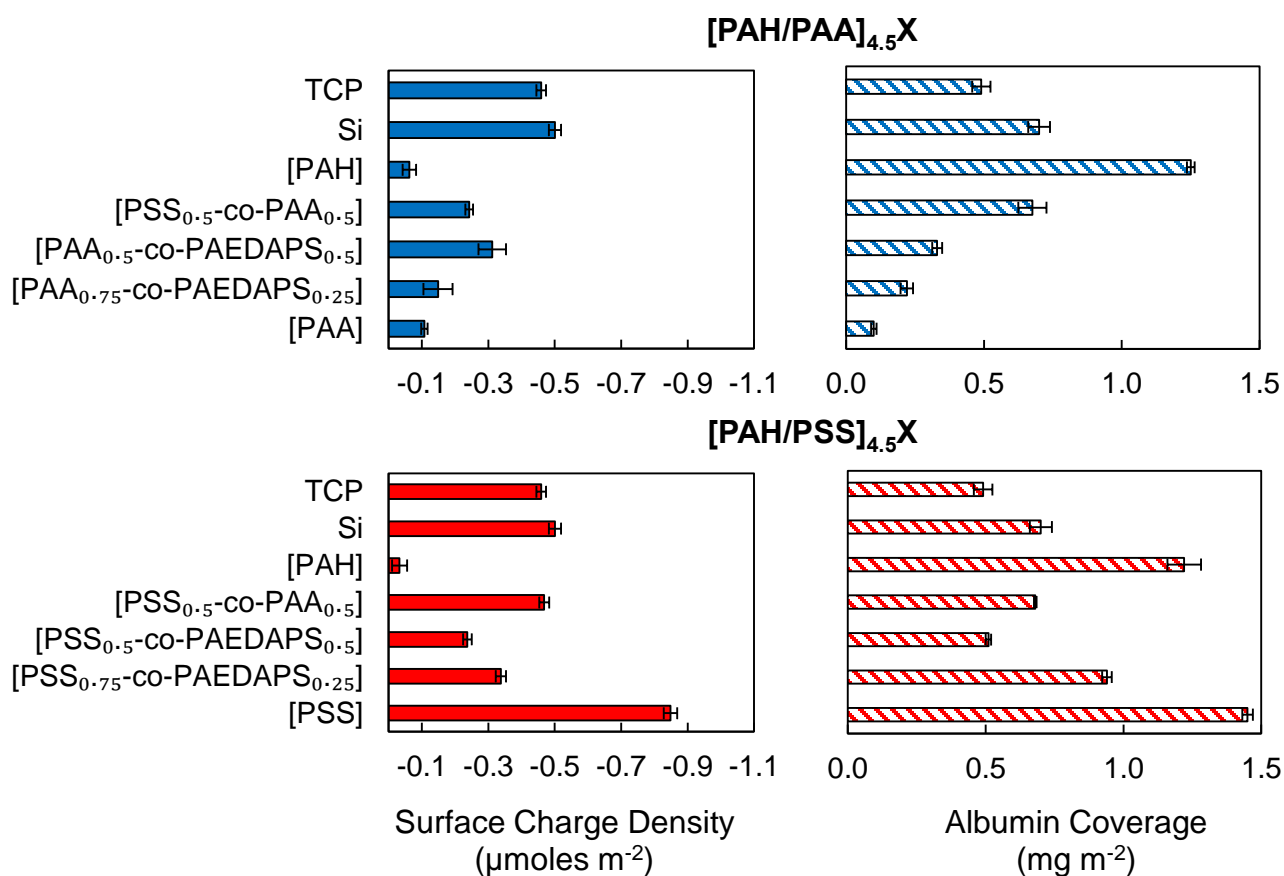
<sup>c</sup> Extent of albumin adsorption: G=good, >0.5 mg m<sup>-2</sup>, P=poor <0.5 mg m<sup>-2</sup>. Cell adhesion G=cells spread and densely packed, P=rounded and sparse,

Figure 1 summarizes the quantitative surface charge density and protein adsorption results for the two base multilayers and the various terminating layers. The control surfaces were tissue culture polystyrene and bare Si wafer. Surface charge density was assayed using radiolabeled (<sup>14</sup>C-) tetraethylammonium cation, shown to displace only surface counterions and not ions within the bulk, termed “extrinsic charge”.<sup>53</sup> An extrinsic charge is a styrene sulfonate or carboxylate repeat unit on PSS or PAA compensated by a counterion. These counterions are displaced when protein adsorbs, providing an entropic driving force for adsorption.<sup>10, 34</sup> The sensitivity of this radiochemical assay of surface charge is good, with a detection limit of about -

$0.1 \times 10^{-6}$  moles charge  $\text{m}^{-2}$ . The technique determines the *exchangeable* surface charge density, a key parameter, given the ion exchange contribution to adsorption.

The use of radiolabeled BSA provides correspondingly low detection limits (about  $0.1 \times \text{mg m}^{-2}$ ) where a monolayer of BSA is approximately  $1.5 \text{ mg m}^{-2}$ .<sup>59</sup> For negative surfaces, Figure 1 reveals a rough correspondence between the extent of surface charge and the amount of protein adsorbed, which is expected if the adsorption mechanism is based on ion displacement of surface cations ( $\text{Na}^+$ ). From prior work on surfaces of controlled charge density, such as mixtures of alkanethiol self-assembled monolayers, the amount of adsorbed protein is known to be correlated to surface charge.<sup>36</sup> The total amount of serum proteins adsorbing to nanoparticles bearing styrene sulfonate surfaces was also reported to increase with charge density.<sup>60</sup>

The PAH (positive) terminated PEMU induces a high amount of protein adsorption, consistent with prior studies.<sup>56, 61</sup> Although the amount of positive charge was not determined here, it was previously discovered that the addition of a polycation to a growing multilayer induces excess polycation throughout the bulk.<sup>53</sup> This “overcompensation” provides extensive material to complex with up to several monolayer equivalents of protein.<sup>39</sup>



**Figure 1.** Negative surface charge density (left) and albumin coverage (right) for [PAH/PAA]<sub>4.5</sub>X and [PAH/PSS]<sub>4.5</sub>X multilayers ending with different polyelectrolytes. Protein adsorbed from 0.1 mg mL<sup>-1</sup> [<sup>125</sup>I]-bovine serum albumin in PBS containing 0.15 M NaCl pH 7.4. Error bars are +/- 1 standard deviation.

Comparing the polyanions and their copolymers in Figure 1 reveals some interesting trends. First, PEMUs terminated with PAA homopolymer produce the lowest surface charge and protein adsorption while PSS induces the highest in both of these parameters. PEMUs terminated with PSS-co-PAA copolymer fall in the intermediate range. Interestingly, the copolymers with zwitterionic repeat unit AEDAPS do not eliminate surface charge and also allow the adsorption of close to a monolayer of BSA when combined with PSS and somewhat less with PAA (Figure 1). Zwitterions have been exploited for their “antifouling” properties, preventing protein and/or cell attachment to surfaces.<sup>10, 37</sup> For complete protein repellency it is likely that dense zwitterion coverage is needed, such as the polymer brush architecture reported by the Jiang group.<sup>62</sup> The surface coverage of 1.45 mg m<sup>-2</sup> BSA obtained on the PSS terminated surface in PBS compares reasonably well with 2.15 mg m<sup>-2</sup> human serum albumin on the same surface measured by Ladam et al.<sup>56</sup>

The control surface, TCP, is polystyrene treated with a plasma to induce carboxylate functionality on the surface.<sup>63, 64</sup> From Figure 1 the TCP surface bears an exchangeable surface charge density of about 0.5 μmol m<sup>-2</sup> leading to about 0.5 mg m<sup>-2</sup> protein adsorption which corresponds to about one third of a monolayer of BSA.<sup>59</sup> Because PAA terminated PEMUs with more than 0.1 μmoles m<sup>-2</sup> PAA on the surface could not be prepared, TCP is used to represent a high charge density carboxylate surface.

### **Fibroblast adhesion: [PAH/PAA]<sub>4.5</sub>X versus [PAH/PSS]<sub>4.5</sub>X**

Many studies of cells growing on multilayers with PAA or PSS (examples in Table S1 Supporting Information) focus on exploring the effect of film stiffness or the sign of the surface charge (terminating layer). Little attention has been given to the chemical functionality that actually provides the charge, perhaps with the assumption that the type of charge is of minor consequence.

The adhesion of 3T3 fibroblasts on [PAH/PAA]<sub>4.5</sub>X and [PAH/PSS]<sub>4.5</sub>X following 3 days of cell culture is compared in Figure 2. The only surface that showed cell culture characteristics (adhesion, spreading and proliferation) as good as those for TCP control was [PAH/PAA]<sub>4.5</sub>PAA (i.e. PAA capping layer on a base PAH/PAA film).<sup>28</sup> Of the remaining surfaces, PAH produced

well spread but sparser populations and also resembled films terminated with the 50/50 copolymer of PAA and PSS. PSS-terminated PEMUs and those copolymers containing PAEDAPS lead to poor attachment and clustering of cells.

Figure 1 shows a correlation between the amount of protein adhesion with charge density, but, for the negative multilayers, comparison of Figure 1 with cell adhesion in Figure 2 immediately reveals a lack of correlation between protein adsorption or surface charge density and cell attachment and spreading. In fact, good adhesion correlates better with *functional group* than with surface charge: carboxylate groups promote adhesion whether they are on top of a multilayer or polystyrene. Films terminated with copolymers having some or all PSS do not encourage cell adhesion. Cells on adhesive surfaces are more elongated and closely packed while those on nonadhesive surfaces are more rounded and sparser.

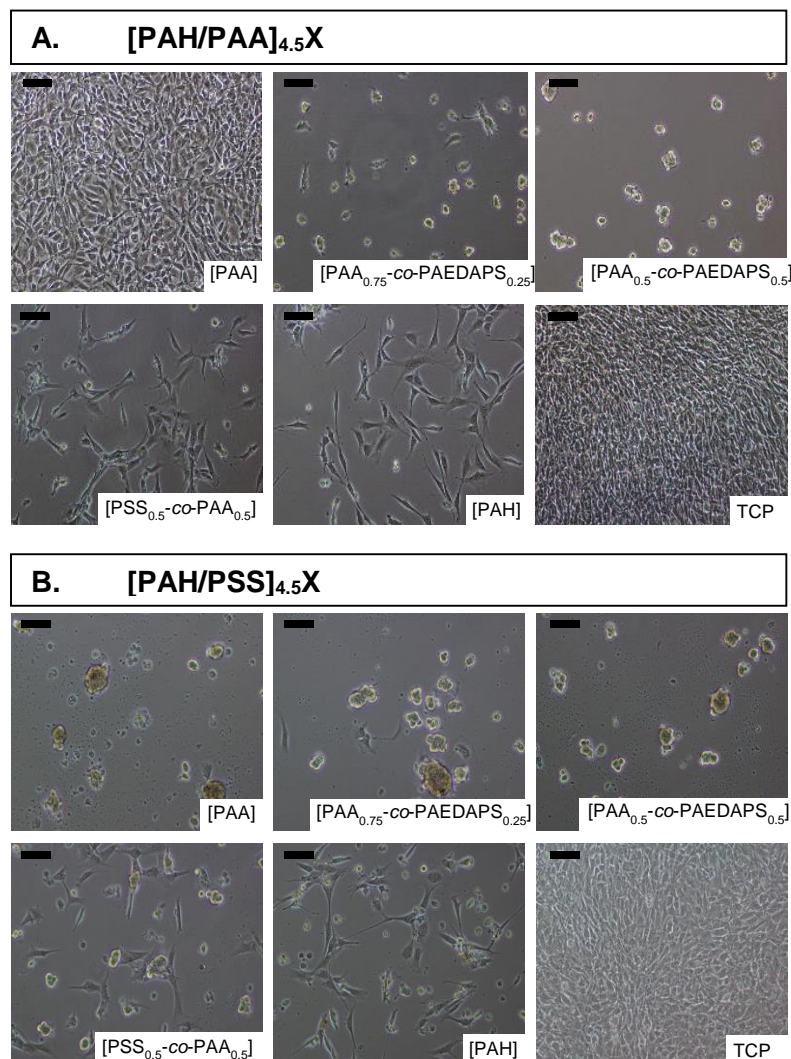


**Figure 2.** Phase contrast micrographs obtained on day 3 of live 3T3 fibroblasts. In image group **A** cells have been seeded on **[PAH/PAA]<sub>4.5</sub>X** multilayers, where **X** is: [PAA]; [PAA<sub>0.75</sub>-co-PAEDAPS<sub>0.25</sub>]; [PAA<sub>0.5</sub>-co-PAEDAPS<sub>0.5</sub>]; [PSS<sub>0.5</sub>-co-PAA<sub>0.5</sub>]; [PAH]; and tissue culture plastic, TCP, control surface. In group **B** cells are seeded on **[PAH/PSS]<sub>4.5</sub>X** multilayers, where **X** is: [PSS]; [PSS<sub>0.75</sub>-co-PAEDAPS<sub>0.25</sub>]; [PSS<sub>0.5</sub>-co-PAEDAPS<sub>0.5</sub>]; [PSS<sub>0.5</sub>-co-PAA<sub>0.5</sub>]; [PAH]. Scale bar 100 μm.

Interestingly, although PAA is the most “cytophilic” surface (using the terminology of Mendelsohn et al.<sup>28</sup>) a slight decrease in interaction strength caused by mixing in zwitterionic functionality turns it “cytophobic.” As seen in Figure 2A, just 25% zwitterion content added to PAA was enough to sharply reduce cell adhesion compared to PAA homopolymer (as seen

previously<sup>55</sup>) whereas the addition of zwitterionic repeat units did not significantly impact the already poor cell adhesion to PSS homopolymer (Figure 2B).

### Comparison of three polyanions [PAH/X]<sub>5</sub> multilayers (X = PAA, PSS and PVS).

In order to focus on the effect of the chemical functionality of the terminating (negative) layer the surface charge densities and albumin coverages for [PAH/X]<sub>5</sub> PEMUs with different polyanions (X = PAA, PSS and PVS) were evaluated (Figure 3). Interestingly, Figure 3 shows that an aromatic sulfonate is more effective than an aliphatic sulfonate at boosting surface charge density, adsorbing albumin, and *preventing* adhesion of fibroblasts to the surface. The carboxylate functionality is again the most effective at *promoting* cell adhesion and spreading. Supporting Information Figure S8 shows that multilayers precoated with albumin induce similar cell morphologies under the same growth conditions.

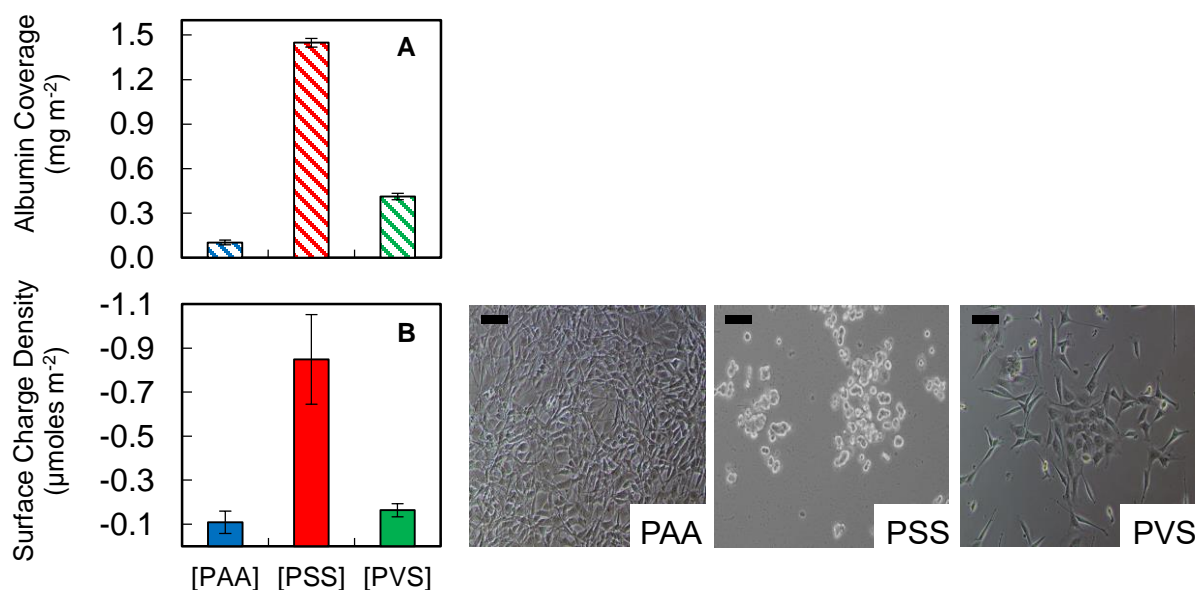


**Figure 3.** (A) Albumin coverage and (B) negative surface charge density data for [PAH/X]<sub>5</sub> multilayers with different polyanions (X = PAA, PSS and PVS 1.0 mM in Tris-buffer 0.15 M NaCl at pH 7.4) and phase contrast micrographs obtained on day 3 of live 3T3 fibroblasts seeded on [PAH/X]<sub>5</sub> multilayers. Scale bar 100 μm.

### Influence of Base layer: [PAH/PAA]<sub>4,5</sub>X and [PAH/PSS]<sub>4,5</sub>X (X = PAA, PSS and PVS).

To verify the base layer had minimal influence on cell adhesion compared to the terminating layer, multilayers  $[\text{PAH}/\text{PAA}]_{4.5}\text{X}$  and  $[\text{PAH}/\text{PSS}]_{4.5}\text{X}$  multilayers were constructed, each ending with PAA, PSS or PVS (Figure 4). For the most part, trends in surface charge and cell adhesion followed those in Figure 3, supporting the idea that the terminating layer controls adhesion. The main exception was the PAH/PSS multilayer terminated with PAA. Figure 4 illustrates somewhat poorer cell spreading on this PEMU compared to one with a PAH/PAA base. It is likely that some localized intermixing has occurred between PSS and PAA at the surface and even a small amount of PSS degrades attachment of cells.

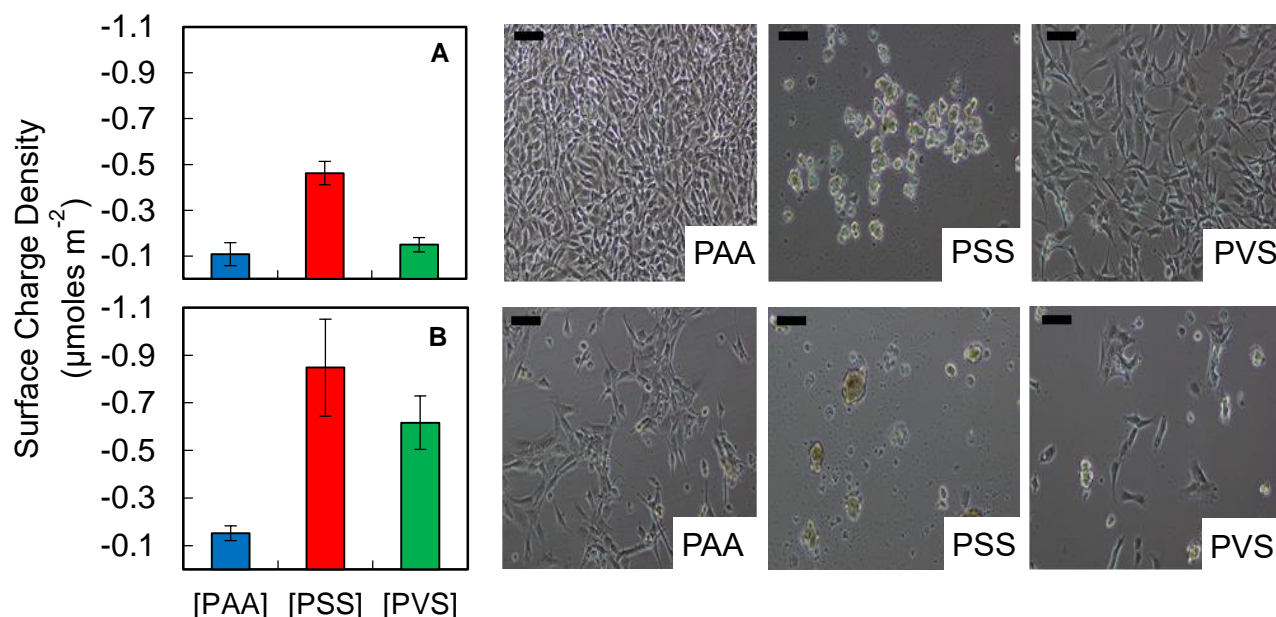


**Figure 4.** Negative surface charge density for (A)  $[\text{PAH}/\text{PAA}]_{4.5}\text{X}$ ; (B)  $[\text{PAH}/\text{PSS}]_{4.5}\text{X}$  multilayers ending with different polyelectrolytes ( $\text{X} = \text{PAA}, \text{PSS}$  and  $\text{PVS}$  1.0 mM in Tris-buffer 0.15 M NaCl pH 7.4) and phase contrast micrographs obtained on day 3 of live 3T3 fibroblasts seeded on  $[\text{PAH}/\text{PAA}]_{4.5}\text{X}$  multilayers on top and  $[\text{PAH}/\text{PSS}]_{4.5}\text{X}$  bottom. Scale bar 100  $\mu\text{m}$ .

### Sulfonate *versus* Carboxylate in Promoting a Hard Corona

The results above illustrate the potentially important difference between deploying sulfonate *versus* carboxylate groups on a surface that is intended to contact physiological environments. The adhesion and proliferation of cells was much better on carboxylate surfaces than on those bearing (aromatic) sulfonates. It is believed the reason for this difference was not related to the amounts of serum albumin coverage, as seen in Figure 1, but to the ease with which the initial serum albumin-rich initial corona could be displaced by cell-adhesive proteins such as

fibronectin. Relative affinities of proteins for surfaces are not well established across different experimental systems, as demonstrated by a recent comprehensive literature survey by Hühn et al.<sup>65</sup> On a molecular scale, the most relevant interactions would be those between a sulfonate or carboxylate and a primary amine such as those found in proteins.

We have recently compared the interaction energies between these anionic repeat units in homopolyelectrolytes with primary amine groups in PAH.<sup>33</sup> In a background salt of KBr the respective interaction energies between PAH and aromatic sulfonates (PSS), aliphatic sulfonates (PVS) and carboxylates (PAA) were -6.34, -3.50 and -2.30 kJ mol<sup>-1</sup>.<sup>33</sup> In NaCl these energies will be higher but in the same order. In other words, the binding strength of aromatic sulfonates to amines is significantly higher than that of carboxylates. In turn, this implies a more exchangeable (softer) corona for carboxylates and the possibility that cell-adhesive proteins will replace the initial albumin on the surface. The soft/reversible nature of PAA/protein interactions has been demonstrated: de Vos et al.<sup>66</sup> and Wittemann et al.<sup>67</sup> showed that BSA desorbs from PAA brushes at concentrations higher than 100 mM on both planar and nanoparticle surfaces, respectively. The differential affinity of proteins for polyelectrolytes has recently been exploited by Bratek-Skicki et al.<sup>68</sup> to separate mixtures of proteins.

Although we were unable to find direct comparisons of sulfonate versus carboxylate in the literature, it appears that in general carboxylate is more frequently deployed on the surface of nanoparticles and planar surfaces. In a closely-related study, Kowalczyńska et al.<sup>69</sup> have compared albumin adsorption and cell adhesion on sulfonated versus unsulfonated (native) polystyrene. Reasoning that adsorbed albumin should discourage adsorption, they used radiolabeled BSA to show that sulfonated polystyrene adsorbs much more BSA and prevents the spreading of the two cells lines employed.

In an effort to quantify the firmness with which albumin is retained on the various surfaces of relevance to this study, radiolabeled BSA was adsorbed to these surfaces and challenged with solutions of increasing displacement strength. The mildest challenge was extended exposure to phosphate buffered saline. The loss of surface BSA was compared to samples challenged with 1.0 M NaCl, which provides a higher ionic strength for stronger ion exchange.<sup>47, 67</sup> The most effective challenge was *via* self-exchange with unlabeled BSA in PBS.

Surfaces selected for comparison included [PAH/PAA]<sub>4,5</sub> capped with PSS, PAA or PVS. Control surfaces were Si wafer, untreated polystyrene (i.e. polystyrene cell culture dish not treated with plasma) and TCP. The coverage of BSA as a function of time was followed after BSA-coated surfaces were immersed in the challenge solutions (Figure S9-14). These kinetic studies indicated that 1 hour was sufficient for the data to reach approximately steady-state values.

Figure 5 compares the results of these challenges. The initial loading of labeled BSA on (unrinsed) surfaces amounted to a 2-3 monolayers. Most of this material was weakly adsorbed. Figure 5 shows TCP and the PAA surfaces retained BSA more weakly. This finding supports the conclusion that sulfonated surfaces form a “harder” corona with BSA compared to carboxylated surfaces. In particular, PAA and TCP retain less than half a monolayer of BSA in PBS.

One monolayer of albumin on silica is about  $1.5 \text{ mg m}^{-2}$  (at pH 7)<sup>70</sup> less than calculated tightly packed monolayer but consistent with the “random sequential adsorption” mechanism for a strongly-adsorbing surface where the immobility of previously adsorbed albumin molecules induces less than close packing (about 54% of close packing in the case of discs).<sup>56</sup>

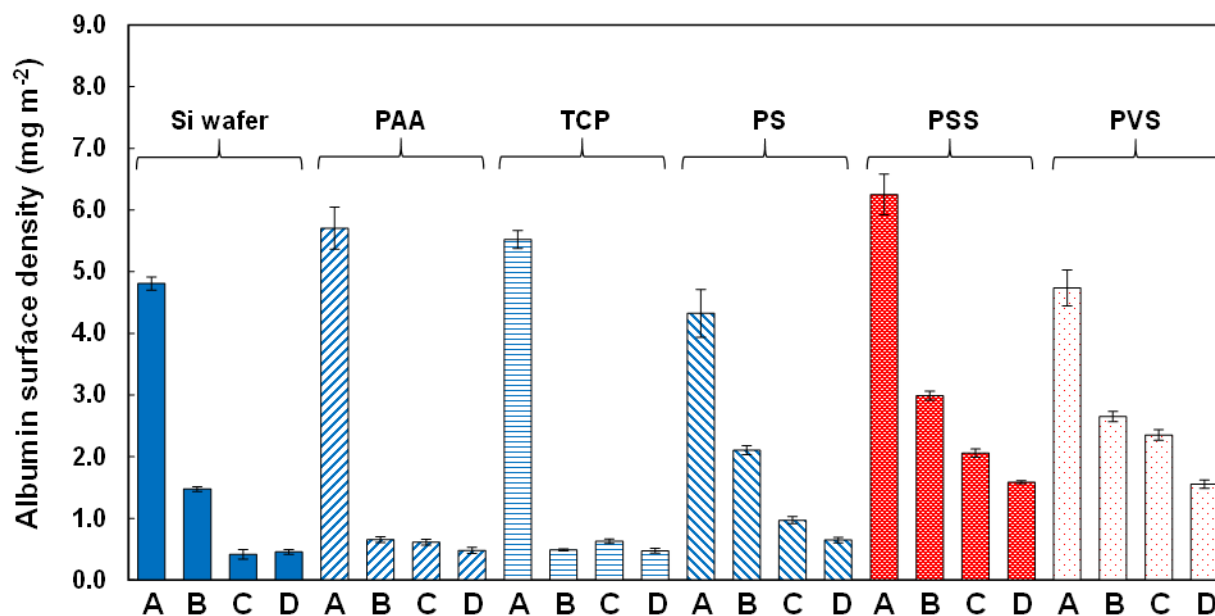


**Figure 5.** Albumin coverage of [<sup>125</sup>I]-BSA on surfaces and multilayers with different terminating layers: (■) Si wafer; (▨) PAA; (▩) TCP; (▧) PS; (▣) PSS; and (▤) PVS. On the x-axis, four adsorption-challenging treatments are specified for each sample: ‘A’ corresponds to albumin coverage after 1 h immersion in  $0.2 \text{ mg mL}^{-1}$  [<sup>125</sup>I]-BSA. ‘B’ corresponds to albumin coverage after 1 h immersion in  $0.2 \text{ mg mL}^{-1}$  [<sup>125</sup>I]-BSA then 100 min in  $0.15 \text{ M NaCl}$  PBS. ‘C’ corresponds to albumin coverage after 1 h immersion in  $0.2 \text{ mg mL}^{-1}$  [<sup>125</sup>I]-BSA then 100 min in  $1.0 \text{ M NaCl}$  in PBS. ‘D’ corresponds to albumin coverage after 1 h immersions in  $0.2 \text{ mg mL}^{-1}$  [<sup>125</sup>I]-BSA then 100 min in  $1\% \text{ BSA}$  in  $0.15 \text{ M NaCl}$  PBS.

### Insight into Protein Adsorption Mechanism

Much of the early understanding of protein adsorption mechanisms has been summarized by Horbett<sup>1, 71</sup> and by Ratner,<sup>24</sup> who also presents some interesting contradictions, paralleled in

the current study. For example, the amount of albumin absorption did not correlate with cell proliferation. Johnson et al. advanced the view that surfaces which held serum albumin too tightly could not be replaced by adhesive proteins.<sup>72</sup>

There was believed to be an optimum range of wettability, around a water contact angle of 50°, for cell adhesion. Arima and Iwata<sup>41</sup> were among many to investigate this idea using well-defined surfaces made from self-assembled monolayers. However, there is no correlation with hydrophobicity in the present work, as PSS terminated PEMUs have a water contact angle of about 25° and PAH/PAA shows a contact angle around 20°. <sup>28</sup> A hydrophilic-hydrophobic comparison using acrylic acid and methylsiloxane surfaces was made by Lassen and Malmsten, who found indications of serum albumin exchange on the former but not on the latter.<sup>73</sup> In a recent study using PEMUs, Guo et al.,<sup>74</sup> investigating the influence of hydrophilicity and charge type, concluded that positive, hydrophilic surfaces lead to the best fibroblast adhesion. However, they only employed carboxylate groups to provide negative charge.

From Figure 1, PSS with a surface sulfonate charge density of  $8.5 \times 10^{-7} \text{ mol m}^{-2}$  retains  $1.45 \text{ mg m}^{-2}$  or  $2.2 \times 10^{-8} \text{ mol m}^{-2}$  albumin. Thus, 38 PSS charges are available for each albumin adsorbed. A combination of random adsorbed coverage (~50% of theoretical monolayer), incomplete access of  $\text{SO}^3$  to albumin, and competition by salt ions for binding sites means not all the polyelectrolyte charges are necessarily bound to proteins. A PAA brush architecture at low ionic strength uses polyelectrolyte charges more efficiently: only 10 charges are needed to immobilize one albumin.<sup>34</sup>

The desirability of depositing a preformed hard *versus* soft corona depends on the application. Clearly, for encouraging cell growth, cell-adhesive proteins must be able to displace enough material directly contacting the surface, unless they can be chemically or strongly physically bound to a hard corona by other mechanisms. This may be why carboxylates are so effective as cell growth surfaces, whether they come from PAA on multilayers or from plasma-deposited carboxylates on plastic. Such a surface could be called biocompatible. On the other hand, if the objective is to passivate a surface, rendering it broadly non-adhesive or antifouling to proteins and platelets, a durable coating of albumin would be desired. Such a surface could *also* be called biocompatible.

## CONCLUSIONS

This work has revealed a difference in cell adhesion correlated to the type of anionic surface charge, which in turn controls the tenacity of serum albumin adsorption. From a practical

standpoint, a coating presenting carboxylate functionality promotes cell adhesion whereas a coating with sulfonate has the opposite effect. While an important distinction between surface charge type has been illustrated here, a number of questions remain open. For example, aromatic and aliphatic sulfonates both strongly retain albumin, yet only aliphatic sulfonates are found naturally. For example, heparin, bristling with anionic charge in the form of carboxylates, sulfates ( $-\text{OSO}_3^-$ ) and aminosulfonate ( $-\text{NH-SO}_3^-$ ), is known to deactivate blood coagulation pathways and has been used extensively for rendering surfaces biocompatible.<sup>26, 75</sup> Solution heparin binds to and activates antithrombin, which down-regulates platelet adhesion and coagulation.<sup>76</sup> Similar mechanisms are thought to operate for heparin coatings.<sup>75</sup> It is possible that this biological inhibition mechanism is supplemented by a broader nonspecific pathway where albumin binds strongly to surface heparin and prevents adhesion of other species in general. It would be interesting to learn if there is an optimum type of sulfonate for albumin trapping. More extensive evaluations of biocompatibility of albumin trapped by sulfonate would include a study of complement and platelet activation as well as discovering whether antibodies are raised against this coating, although this latter possibility is unlikely as long as the albumin remains in a form approximating its native state. In addition, it would be interesting to evaluate the corona composition after a sulfonate-terminated surface is introduced *in vivo*. If the composition of the sulfonate-locked corona mirrors that of the naturally-occurring plasma it would be an important step to “personalizing” the corona to that of the host.

## ASSOCIATED CONTENT

### Supporting Information

<sup>1</sup>H-NMR of copolymers, polymerizations monitored by <sup>1</sup>H-NMR; calibration curves for radiolabeled BSA coverage; cell growth on surfaces pretreated with albumin, surface charge films before and after treatment with PBS; Table summarizing literature findings on cells adhesion to multilayers,

## AUTHOR INFORMATION

### Corresponding Author

\*E-mail: schlen@chem.fsu.edu

### Notes

The authors declare no competing financial interest.

**Acknowledgements** This work was supported in part by a grant from the National Science Foundation (DMR-1506824), and by the Florida State University.

## REFERENCES

1. T. A. Horbett, *Colloids Surf. B*, 1994, **2**, 225-240.
2. L. Vroman and A. L. Adams, *Surf Sci*, 1969, **16**, 438-446.
3. E. Casals, T. Pfaller, A. Duschl, G. J. Oostingh and V. Puentes, *ACS Nano*, 2010, **4**, 3623-3632.
4. T. Cedervall, I. Lynch, S. Lindman, T. Berggård, E. Thulin, H. Nilsson, K. A. Dawson and S. Linse, *Proc. Natl. Acad. Sci. U. S. A.*, 2007, **104**, 2050-2055.
5. D. Walczyk, F. B. Bombelli, M. P. Monopoli, I. Lynch and K. A. Dawson, *J. Am. Chem. Soc.*, 2010, **132**, 5761-5768.
6. S. Schöttler, K. Landfester and V. Mailänder, *Angew. Chem. Int. Ed.*, 2016, **55**, 8806-8815.
7. T. A. Horbett, *Colloids Surf. B: Biointerfaces*, 1994, **2**, 225-240.
8. M. L. Immordino, F. Dosio and L. Cattel, *Int. JNnanomed.*, 2006, **1**, 297-315.
9. J. V. Jokerst, T. Lobovkina, R. N. Zare and S. S. Gambhir, *Nanomedicine*, 2011, **6**, 715-728.
10. J. B. Schlenoff, *Langmuir*, 2014, **30**, 9625-9636.
11. S. Schöttler, G. Becker, S. Winzen, T. Steinbach, K. Mohr, K. Landfester, V. Mailänder and F. R. Wurm, *Nat. Nanotechnol.*, 2016, **11**, 372.
12. M. A. Dobrovolskaia, B. W. Neun, S. Man, X. Ye, M. Hansen, A. K. Patri, R. M. Crist and S. E. McNeil, *Nanomed.: Nanotechnol. Biol. Med.*, 2014, **10**, 1453-1463.
13. S. Schöttler, K. Landfester and V. Mailänder, *Angew. Chem. Int. Edit.*, 2016, **55**, 8806-8815.
14. C. Tao, Y. J. Chuah, C. Xu and D.-A. Wang, *J. Mater. Chem. B*, 2019, **7**, 357-367.
15. S. Seneca, J. Simon, C. Weber, A. Ghazaryan, A. Ethirajan, V. Mailänder, S. Morsbach and K. Landfester, *Macromol. Biosci.*, 2018, **18**, 1800075.
16. A. Poot, T. Beugeling, J. P. Cazenave, A. Bantjes and W. G. van Aken, *Biomaterials*, 1988, **9**, 126-132.
17. M. Amiji and K. Park, *J. Biomater. Sci. Polym. Ed.*, 1993, **4**, 217-234.
18. C. D. McFarland, C. De Filippis, M. Jenkins, A. Tunstall, N. P. Rhodes, D. F. Williams and J. G. Steele, *J. Biomater. Sci. Polym. Ed.*, 1998, **9**, 1227-1239.
19. B. Yang, J. C. Kim, J. Seong, G. Tae and I. Kwon, *Biomater Sci*, 2018, **6**, 2092-2100.
20. A. M. Makhson, B. Afanasyev, G. M. Manikhas, M. J. Hawkins, M. R. Green, P. Bhar and S. Orlov, *Ann. Oncol.*, 2006, **17**, 1263-1268.
21. Q. Peng, S. Zhang, Q. Yang, T. Zhang, X.-Q. Wei, L. Jiang, C.-L. Zhang, Q.-M. Chen, Z.-R. Zhang and Y.-F. Lin, *Biomaterials*, 2013, **34**, 8521-8530.
22. Z. Li, D. Li, Q. Li, C. Luo, J. Li, L. Kou, D. Zhang, H. Zhang, S. Zhao, Q. Kan, J. Liu, P. Zhang, X. Liu, Y. Sun, Y. Wang, Z. He and J. Sun, *Biomater Sci*, 2018, **6**, 2681-2693.
23. M. Rabe, D. Verdes and S. Seeger, *Adv Colloid Interfac*, 2011, **162**, 87-106.
24. C. D. Tidwell, S. I. Ertel, B. D. Ratner, B. J. Tarasevich, S. Atre and D. L. Allara, *Langmuir*, 1997, **13**, 3404-3413.
25. J. H. Ryu, P. B. Messersmith and H. Lee, *ACS Appl Mater. Interfac.*, 2018, **10**, 7523-7540.
26. I. You, S. M. Kang, Y. Byun and H. Lee, *Bioconjugate Chem*, 2011, **22**, 1264-1269.
27. G. Decher and J. B. Schlenoff, *Multilayer Thin Films: Sequential Assembly of Nanocomposite Materials*, 2nd Ed., Wiley-VCH, Weinheim, 2012.
28. J. D. Mendelsohn, S. Y. Yang, J. Hiller, A. I. Hochbaum and M. F. Rubner, *Biomacromolecules*, 2003, **4**, 96-106.
29. V. Gribova, R. Auzely-Velty and C. Picart, *Chem. Mater.*, 2012, **24**, 854-869.

30. Z. Y. Tang, Y. Wang, P. Podsiadlo and N. A. Kotov, *Adv. Mater*, 2006, **18**, 3203-3224.
31. J. M. Levasalmi and T. J. McCarthy, *Macromolecules*, 1997, **30**, 1752-1757.
32. D. Yoo, S. S. Shiratori and M. F. Rubner, *Macromolecules*, 1998, **31**, 4309-4318.
33. J. Fu, H. M. Fares and J. B. Schlenoff, *Macromolecules*, 2017, **50**, 1066-1074.
34. X. Xu, S. Angioletti-Uberti, Y. Lu, J. Dzubiella and M. Ballauff, *Langmuir*, 2019, **35**, 5373-5391..
35. A. Gessner, A. Lieske, B. R. Paulke and R. H. Müller, *Europ. J. Pharm. Biopharm.*, 2002, **54**, 165-170.
36. E. Beurer, N. V. Venkataraman, M. Sommer and N. D. Spencer, *Langmuir*, 2012, **28**, 3159-3166.
37. S. Jiang and Z. Cao, *Adv. Mater.*, 2010, **22**, 920-932.
38. J. D. Delgado and J. B. Schlenoff, *Macromolecules*, 2017, **50**, 4454-4464.
39. D. S. Salloum and J. B. Schlenoff, *Biomacromolecules*, 2004, **5**, 1089-1096.
40. C. J. Arias, T. C. S. Keller and J. B. Schlenoff, *Langmuir*, 2015, **31**, 6436-6446.
41. Y. Arima and H. Iwata, *Biomaterials*, 2007, **28**, 3074-3082.
42. J. T. Parsons, A. R. Horwitz and M. A. Schwartz, *Nat. Rev. Mol. Cell Biol.*, 2010, **11**, 633.
43. D. Fischer, Y. Li, B. Ahlemeyer, J. Krieglstein and T. Kissel, *Biomaterials*, 2003, **24**, 1121-1131.
44. E. Yavin and Z. Yavin, *J. Cell Biol.*, 1974, **62**, 540-546.
45. T. Peters, *All About Albumin: Biochemistry, Genetics, and Medical Applications*, Academic Press, San Diego, 1995.
46. L. Shang and G. U. Nienhaus, *Acc. Chem. Res.*, 2017, **50**, 387-395.
47. A. Brooks C and M. Cramer S, *AIChE J.*, 1992, **38**, 1969-1978.
48. G. A. Kulikova, I. V. Ryabinina, S. S. Guseynov and E. V. Parfenyuk, *Thermochim. Acta*, 2010, **503**, 65-69.
49. C. F. Amstein and P. A. Hartman, *J Clin Microbiol*, 1975, **2**, 46-54.
50. S. I. Ertel, B. D. Ratner and T. A. Horbett, *J. Biomed. Mater. Res.*, 1990, **24**, 1637-1659.
51. A. Buxboim, I. L. Ivanovska and D. E. Discher, *J Cell Sci*, 2010, **123**, 297-308.
52. S. Mehrotra, S. C. Hunley, K. M. Pawelec, L. Zhang, I. Lee, S. Baek and C. Chan, *Langmuir*, 2010, **26**, 12794-12802.
53. R. A. Ghostine, M. Z. Markarian and J. B. Schlenoff, *J. Am. Chem. Soc.*, 2013, **135**, 7636-7646.
54. C. J. Arias, R. L. Surmaitis and J. B. Schlenoff, *Langmuir*, 2016, **32**, 5412-5421.
55. S. G. Olenych, M. D. Moussallem, D. S. Salloum, J. B. Schlenoff and T. C. S. Keller, *Biomacromolecules*, 2005, **6**, 3252-3258.
56. G. Ladam, C. Gergely, B. Senger, G. Decher, J. C. Voegel, P. Schaaf and F. J. G. Cuisinier, *Biomacromolecules*, 2000, **1**, 674-687.
57. J. Romanowska, D. B. Kokh and R. C. Wade, *Nano Lett.*, 2015, **15**, 7508-7513.
58. Y. Luan, D. Li, Y. Wang, X. Liu, J. L. Brash and H. Chen, *Langmuir*, 2014, **30**, 1029-1035.
59. C. E. Giacomelli and W. Norde, *J. Coll. Interfac. Sci.*, 2001, **233**, 234-240.
60. A. Gessner, A. Lieske, B. R. Paulke and R. H. Müller, *Eur. J. Pharm. Biopharm.*, 2002, **54**, 165-170.
61. J.-H. Lin, H.-Y. Chang, W.-L. Kao, K.-Y. Lin, H.-Y. Liao, Y.-W. You, Y.-T. Kuo, D.-Y. Kuo, K.-J. Chu, Y.-H. Chu and J.-J. Shyue, *Langmuir*, 2014, **30**, 10328-10335.
62. Z. Zhang, T. Chao, S. Chen and S. Jiang, *Langmuir*, 2006, **22**, 10072-10077.
63. C. F. Amstein and P. A. Hartman, *J. Clin. Microbiol.*, 1975, **2**, 46.
64. S. I. Ertel, B. D. Ratner and T. A. Horbett, *J. Biomed. Mater. Res. A*, 1990, **24**, 1637-1659.
65. J. Hühn, C. Fedeli, Q. Zhang, A. Masood, P. del Pino, N. M. Khashab, E. Papini and W. J. Parak, *Int. J. Biochem. Cell Biol.*, 2016, **75**, 148-161.
66. W. M. de Vos, P. M. Biesheuvel, A. de Keizer, J. M. Kleijn and M. A. Cohen Stuart, *Langmuir*, 2008, **24**, 6575-6584.
67. A. Wittemann, B. Haupt and M. Ballauff, *PCCP*, 2003, **5**, 1671-1677.

68. A. Bratek-Skicki, V. Cristaudo, J. Savocco, S. Nootens, P. Morsomme, A. Delcorte and C. Dupont-Gillain, *Biomacromolecules*, 2019, **20**, 778-789.
69. H. M. Kowalczyńska, M. Nowak-Wyrzykowska, A. A. Szczepankiewicz, J. Dobkowski, M. Dyda, J. Kamiński and R. Kołos, *Coll.Surf. B: Biointerfac.*, 2011, **84**, 536-544.
70. K. Nakanishi, T. Sakiyama and K. Imamura, *J. Biosci. Bioeng.*, 2001, **91**, 233-244.
71. T. A. Horbett, *J. Biomed. Mater. Res.*, 1981, **15**, 673-695.
72. D. Johnson S, M. Anderson J and E. Marchant R, *J. Biomed. Mater. Res.*, 1992, **26**, 915-935.
73. B. Lassen and M. Malmsten, *J. Coll. Interfac. Sci.*, 1997, **186**, 9-16.
74. S. Guo, X. Zhu, M. Li, L. Shi, J. L. T. Ong, D. Jańczewski and K. G. Neoh, *ACS Appl. Mater. Interfac*, 2016, **8**, 30552-30563.
75. J. Andersson, J. Sanchez, K. N. Ekdahl, G. Elgue, B. Nilsson and R. Larsson, *J. Biomed. Mater. Res. A*, 2003, **67A**, 458-466.
76. S. T. Olson, I. Björk and J. D. Shore, in *Methods in Enzymology*, Academic Press, 1993, vol. 222, pp. 525-559.

Graphical Abstract FOR PUBLICATION ONLY

